Cancer Letters 446 (2019) 25–37

Contents lists available at ScienceDirect

Cancer Letters

journal homepage: www.elsevier.com/locate/canlet

Original Articles

Cell-targeted c(AmpRGD)-sunitinib molecular conjugates impair tumor growth of melanoma

Francesca Bianchini[a,*], Elisabetta Portioli[b], Francesca Ferlenghi[b], Federica Vacondio[b], Elena Andreucci[a], Alessio Biagioni[a], Jessica Ruzzolini[a], Silvia Peppicelli[a], Matteo Lulli[a], Lido Calorini[a], Lucia Battistini[b], Franca Zanardi[b], Andrea Sartori[b,**]

[a] Department of Experimental and Clinical Biomedical Sciences "Mario Serio", University of Florence, Viale Morgagni 50, 50134, Florence, Italy
[b] Food and Drug Department, University of Parma, Parco Area delle Scienze 27A, 43124, Parma, Italy

ARTICLE INFO

Keywords:
Multi-targeting drugs
RTK inhibitors
Integrin ligands
Selective cell-internalization

ABSTRACT

Drug resistance and off-organ toxicity remain unsolved issues in chemotherapy of advanced-stage melanoma patients. Thus, the creation of new molecular conjugates able to combine a selective accumulation, high ability of internalization and signaling pathway inhibition, are highly requested. Recently, we reported a new class of molecular conjugates, compounds **1–3**, where the anti-$\alpha_V\beta_3$ integrin peptidomimetic c(AmpRGD), which is a selective ligand for $\alpha_V\beta_3$ integrin, was covalently bound to the tyrosine kinase inhibitor sunitinib. Here, we report that these c(AmpRGD)-sunitinib conjugates and, in particular, compound **3**, are selectively internalized by human melanoma cells through $\alpha_V\beta_3$ receptor-mediated endocytosis. Compound **3** is more effective than sunitinib in reducing *in vitro* melanoma cells proliferation, cloning efficiency, migration, and invasion. More interestingly, compound **3** is able to significantly reduce the growth of xenografted melanoma tumor developed in immune-compromised mice, more efficiently than an equimolar dose of sunitinib. Indeed, its targeting ability was demonstrated by the selective localization at the tumor level with respect to healthy tissues. Thus, c(AmpRGD)-sunitinib conjugates such as compound **3** could serve as intriguing multiple-target agents to selectively reach melanoma cells and interfere with the progression of the disease.

1. Introduction

Melanoma is one of the most aggressive forms of skin cancer diagnosed in people, especially those aged 55–64 years. In the past few decades, the global incidence of melanoma has continuously increased and it is expected to grow further in the next years, making melanoma a serious threat to public health [1–4]. Cancer stage at diagnosis determines treatment options and dictates the length of patient survival. Thus, for localized melanoma lesions (covering about 83% of all cases) surgery represents the conventional and most effective treatment, resulting in more than 98% survival over 5-years, while advanced-stage unresectable or metastatic melanoma involving metastases to regional or distant lymph nodes and/or other sites is generally associated with poor prognosis and short-term survival [5,6].

Before 2011, metastatic melanoma was considered an almost incurable disease, and standard-of-care treatment met only modest clinical benefit by the use of untargeted chemotherapy (dacarbazine) and/or untargeted immunotherapy (interferon and interleukin cytokines). The median overall survival obtained was of 9 months and substantial toxicity was often recorded [7,8]. In-depth, decade-long research into the genomics of cancer and underpinnings of the immune response against cancer changed the shape of the frontline treatment of advanced stage melanomas, with about ten new therapeutic agents having been approved since 2011 by FDA and homologous agencies for the effective treatment of metastatic melanoma [9,10].

In particular, the discovery that about half of all melanomas harbor *BRAF* mutations, with the most common oncogenic event involving the V600E mutation in BRAF protein, paved the way to the medicinal chemistry-driven generation of molecularly targeted small molecules, such as vemurafenib and dabrafenib, as potent and specific inhibitors of V600-mutated BRAF [11–16]. Soon after, the appreciation that BRAF signaling is dependent on downstream activation of MEK1/2, and the need of overcoming mechanisms of resistance to BRAF inhibitors, led to the development of small molecule MEK-inhibitors trametinib and

* Corresponding author. Department of Experimental and Clinical Biomedical Science, University of Florence, Viale GB Morgagni 50, 50134 Firenze, Italy.
** Corresponding author. Food and Drug Department, University of Parma, Parco Area delle Scienze 27A, 43124, Parma, Italy.
E-mail addresses: francesca.bianchini@unifi.it (F. Bianchini), andrea.sartori@unipr.it (A. Sartori).

https://doi.org/10.1016/j.canlet.2018.12.021
Received 24 July 2018; Received in revised form 5 October 2018; Accepted 31 December 2018

cobimetinib, approved as monotherapy or, better, in combination with BRAF inhibitors.

Concurrently, the introduction of immunotherapeutic approaches using targeted immune checkpoint inhibitors, such as monoclonal antibodies ipilimumab or nivolumab, has demonstrated substantial improvement in survival in patients with metastatic disease to at least two years [17,18].

Despite progress in the clinical management of advanced-stage melanoma with different treatment options available, mainly based on consideration of patient-specific features (presence of genetic modifications, kinetics of melanoma, performance status, comorbidities, baseline immune recognition, etc.), many concerns still exist dealing with the observed overall toxicity [19,20], the effective dosing regimens and, above all, the insurgence of resistance mechanisms leading to tumor relapse and progression to a metastatic disease with incredibly aggressive features [21].

Given the involvement of multiple, yet strictly related biological targets and signaling cascades in the metastatic melanoma disease, the combination therapy has become the standard-of-care treatment, in both small molecule-based (e.g. vemurafenib + cobinetinib in $BRAF^{V600E/K}$-mutant disease) and antibody-based therapies (e.g. ipilimumab + nivolumab), with the primary goal to improve clinical benefit while overcoming the insurgence of drug resistance and compensating mechanisms often observed using targeted monotherapy.

In these cases, however, off-organ (and possible synergistic) toxicity remains a still unsolved issue, mainly due to the fact that *molecularly-targeted compounds* may be *cell-unselective*, at least when the biological target is located inside cells. On the other hand, large-size drugs such as antibodies selectively addressing extracellular biological targets are not amenable to target intracellular proteins.

The creation of *new molecular conjugates* which combine in a sole chemical entity, i) the capability of accumulating in melanoma cells in a target-selective manner by recognition of specific surface-exposed receptors, ii) the ability to enter cells, possibly via receptor-mediated endocytosis, iii) the capacity to modulate key intracellular targets and signaling pathways, is an appealing approach toward enhanced drug efficacy at a lowered drug dosage with an increased safety window [22,23].

Recently, we reported a new class of molecular conjugates, compounds **1–3**, where the anti-$\alpha_V\beta_3$ integrin peptidomimetic c(AmpRGD) [24–28] was connected to the antiangiogenic and antitumor multikinase inhibitor sunitinib through robust linkers (Fig. 1). The rationale behind this work was that the c(AmpRGD) portion would have selectively directed the conjugates toward $\alpha_V\beta_3$-integrin overexpressing cells (including activated endothelial, melanoma, ovarian, pancreatic, cervical and breast carcinoma, glioblastoma cells) [29], while the sunitinib moiety would have exerted its anti-angiogenic properties through its proven ability to inhibit key intracellular tyrosine kinases including tumor angiogenesis-related VEGFR-2 receptor [30–33]. We demonstrated, using both *in vitro* and *in vivo* protocols, that the robust chemical association and co-localization of the two modules – c(AmpRGD) and sunitinib - increased the capacity to interfere with the synergetic interactions that follow the crosstalk between the $\alpha_V\beta_3$ integrin receptor and VEGFR, thus impairing tumor-associated angiogenesis [28].

Based on the above considerations, we wondered whether these three conjugates **1–3** could serve as intriguing multiple-target agents to selectively reach melanoma cells and interfere with the progression of metastatic melanoma.

In this work, the effect of these different c(AmpRGD)-sunitinib chemotypes – compounds **1–3** – on a preclinical model of advanced human melanoma cells has been evaluated. In addition, rationalization of the observed cell-selective effects has been proposed, based on the multi-targeting activity of these molecular conjugates as both RTK inhibitors and $\alpha_V\beta_3$ antagonists. We found that, among these c-AmpRGD-sunitinib conjugates, compound **3**, i) is selectively internalized by human melanoma cells through $\alpha_V\beta_3$ receptor-mediated endocytosis, ii) it is more effective than sunitinib in reducing *in vitro* melanoma cells proliferation, cloning efficiency, migration and invasion, and iii) it is able to significantly reduce growth of xenografted melanoma tumor developed in immune-compromised mice, more efficiently than an equimolar dose of sunitinib.

2. Materials & methods

2.1. Synthesis

The molecular conjugates **1–3** and the reference compound c(AmpRGD)-NH_2 (**4**) (Fig. 1) were prepared according to the procedure reported in Ref. [28]. The sunitinib reference (as sunitinib malate salt) was purchased by LC Laboratories (USA) with a purity of > 99%.

2.2. pKa determination

The pKa values of sunitinib and compounds **1–3** were determined by the potentiometric pH-metric method employing a Sirius T3 instrument (Sirius Analytical Ltd, Forrest Row, UK). The detailed experimental procedure is reported in the Supporting Information [34,35].

2.3. Cell cultures

The human melanoma cell line (M21), human prostate carcinoma cell line (PC3), and human erythroleukemia cell line K562 were purchased from the American Type Culture Collection (ATCC, Rockville, MD). M21 and PC3 were grown in Dulbecco's modified Eagle medium, containing 4500 mg/L glucose (DMEM 4500, GIBCO) supplemented with 10% fetal calf serum (FCS) at 37 °C in a humidified incubator containing 10% CO_2. 5.0×10^5 melanoma cells or prostate carcinoma cells were seeded in 100 mm Sarstedt dishes and propagated every 3 days by incubation with a trypsin–EDTA solution. The human erythroleukemia cell line K562 was maintained at 37 °C in Iscove's Modified Dulbecco's Medium (IMDM, GIBCO) supplemented with 10% FCS in T25 culture flasks (Sarstedt) in a humidified incubator with 5% CO_2. When cultures reached a cell density between 1×10^5 and 1×10^6 cells/mL, cells were resuspended in warm fresh media at a volume to yield a density of 2×10^5 cells/mL. M21, PC3, and K562 cultures were periodically monitored for mycoplasma contamination using Chen's fluorochrome test [36].

The expression levels of $\alpha_V\beta_3$ integrin receptor on M21, PC3, and K562 cell lines were confirmed by flow cytometric analysis [37,38].

2.4. Inhibition of cell adhesion to vitronectin

96 wells plates were coated with vitronectin (10 μg/mL) (V8379 Sigma) by overnight incubation at 4 °C. Plates were washed with Phosphate Buffered Saline (PBS) solution and then incubated at 37 °C for 1 h with PBS containing 1% Bovine Serum Albumin (BSA). M21 cells were washed by centrifugation with PBS, counted and suspended in serum-free medium at 0.6×10^6 cells/mL. Melanoma cell suspensions were exposed to different amounts of the compounds **1–4** (final concentration ranged from 30 μM to 10 nM), while prostate carcinoma (PC3) and erythroleukemia (K562) cells were exposed to different concentrations of c(AmpRGD)-NH_2 (**4**). A pre-incubation at 37 °C for 30 min was performed to allow the ligand-receptor equilibrium to be reached. Assays were performed in the presence of 2 mmol/L $MnCl_2$. Cells were then plated on VN substrata ($5–6 \times 10^4$ cells/well) and incubated at 37 °C for 1 h. Plates were washed with PBS to remove the non-adherent cells, and 200 μL of 0.5% crystal violet solution in 20% methanol were added. After 2 h of incubation at 4 °C, plates were examined at 540 nm in a counter ELX800 (Bio TEK Instruments). Experiments were conducted in triplicate and repeated at least three times. The values are expressed as % inhibition ± SEM of cell adhesion relative to untreated cells.

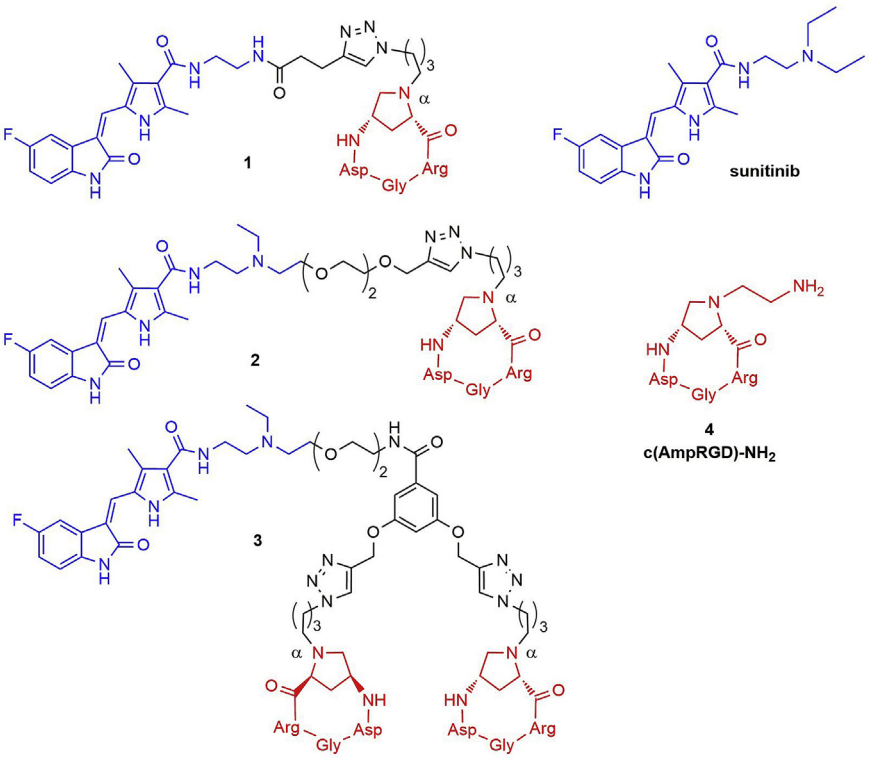

Fig. 1. Molecular structures of c(AmpRGD)-sunitinib conjugates **1–3**, antiangiogenic drug sunitinib, and c(AmpRGD)-NH_2 **4**.

2.5. Clonogenic assay

M21 cells were exposed to different treatments for 24 h and then seeded at low density (200 cells in 60 mm diameter Petri dishes) in growth medium supplemented with 10% FCS. Cultures were grown for 14 days at 37 °C in a humidified incubator. Growth medium was changed every 3–4 days. After 2 weeks, the clones were fixed with 4% formaldehyde and stained with 0.1% crystal violet. In some experiments, M21 cells were exposed for 6 days to different treatments (every other day) and then seeded at low density in growth medium supplemented with 10% FCS. Cultures were grown for 14 days at 37 °C in a humidified incubator and treated every other day with different treatments and the medium was changed. After 2 weeks, the clones were fixed with 4% formaldehyde and stained with 0.1% crystal violet. Cell clones with diameter > 0.5 mm were counted under an optical microscope (10 × magnification) and the surviving factor (SF) was calculated on the basis of the following formulas: cloning efficiency (CE) (%) = (number of clones formed from untreated cells/number of untreated cells inoculated) × 100%; surviving factor (SF): (number of clones from treated cells)/(treated cells seeded × CE) [39]. Proliferation and clonogenic assays were carried out in triplicate and repeated a minimum of 3 times independently.

2.6. Evaluation of cell internalization of sunitinib and compounds 1–3

Internalization of sunitinib was determined by taking advantage of the fluorescent emission of sunitinib by means of a cytofluorimetric assay and immunofluorescence analysis. Briefly, M21 cells were seeded in standard medium (2×10^6 cells/100 mm Petri dishes) and after 24 h adhesion cells were exposed to sunitinib or compounds **1–3** at 1 μM concentration. After 24 h, cells were gently detached using Accutase (Lonza) and the fluorescence associated with different cell populations was evaluated using the FITC channel of the FACSCanto BD instrument. Untreated cells were used as negative control. For cell selective internalization experiments 1×10^6 M21 human melanoma cells were seeded in complete medium in 60 mm dishes and, after 3 h of adhesion, 1×10^6 K562 erythroleukemia cells were stratified on M21 cell monolayers in 1:1 ratio. M21, K562, and M21:K562 cell cultures were exposed to different treatments with sunitinib or compounds **1–3** at 1 μM concentration for 24 h. After incubation, adherent and non-adherent cells were recovered and washed in PBS, and incubated for 1 h at 4 °C in the presence of anti-$\alpha_V\beta_3$ monoclonal antibody (1 μg/50 μL) (clone LM609, Millipore). Cells were then washed and incubated for 1 h at 4 °C with a specific secondary antibody, goat antimouse IgG conjugated with Cy5 (AbCam) for cytofluorimetric analysis.

For immunofluorescence assay M21 cells (2×10^5 cells) were seeded on vitronectin-coated (2 μg/mL) 25-mm cover glasses, at the bottom of 60 mm dishes, in complete medium, and allowed to grow for 24 h. Cells were successively exposed to different compounds (1 μM) for 24 h. At the end of the incubation, cells were fixed for 20 min in 4% paraformaldehyde. For displacement experiments, M21 cells were exposed to 10 μM concentration of reference compound **4** (2 h) before treatment with compound **3** at 1 μM concentration for 24 h.

In some experiments (localization), cells were permeabilized with 0.1% Triton X-100 solution in PBS and incubated in blocking solution (PBS supplemented with 4% BSA and 1% horse serum) and then incubated overnight at 4 °C with the anti-Rab7 antibody (Santa Cruz sc-376362). Cells were washed and then incubated for 1 h using 1:100 goat anti-rabbit IgG-Cy3. Cell nuclei were counterstained with DAPI (4′,6-diamidino-2-phenylindole; Life Technologies) (1 μg/mL for 10 min). Following two washes in PBS, coverslips were mounted with 1:1 PBS:Glycerol on glass slides and the cells were observed with an inverted confocal Nikon Eclipse TE2000 microscope equipped with a 960S-Fluor oil immersion lens (FITC filter for sunitinib, Cy3 filter for Rab-7, DAPI filter for nuclear stain) [40]. A single composite image was obtained by superimposition of 6 optical sections for each sample observed.

2.7. Western blot assay

M21 cells were exposed for 24 h to serum-free medium for starvation. Next, 1 μM concentration of different compounds was added to cell monolayers. After 1 h incubation, media were rapidly removed and cell monolayers were exposed to (100 μL/p100 diameter dishes) RIPA lysis buffer (50 mM Tris pH 7.4, 150 mM NaCl, 1% Triton X-100, 1% sodium deoxycholate, 0.1% SDS, 5 mM EDTA) and proteinase inhibitor cocktail (Roche, Mannheim, Germany) for 30 min in ice. Lysates were then centrifuged at 14,000 r.p.m. for 20 min and the supernatants were collected and stored at −80 °C. Protein content was quantified by the Bradford method (Bio-Rad, Hercules, CA). Fifty to 60 μg of total proteins were denaturated at 90 °C for 5 min in Laemmli buffer and separated on Bolt® Bis-Tris Plus gels 4–12% precast polyacrylamide gels (Life Technologies, Monza, Italy). Fractionated proteins were transferred from the gel to a PVDF nitrocellulose membrane using the iBlot 2 system (Life Technologies, Monza, Italy). Membranes were blocked for 1 h, at room temperature, with Odyssey blocking buffer (Dasit Science, Cornaredo, MI, Italy). Subsequently, the membranes were probed at 4 °C overnight with appropriate primary antibodies diluted in a solution of 1:1 Odyssey blocking buffer/T-PBS buffer, washed four times with PBS-Tween 0.1% solution, and probed with the secondary IRDye antibodies according to the manufacturer's instructions. The protein bands were analyzed by the Odyssey Infrared Imaging System (Lycor Bioscience) using software for protein quantification. The primary antibodies were: rabbit anti-pERK (1:1000, #4370 Cell Signaling Technology), rabbit anti-ERK (1:1000, #4695 Cell Signaling Technology), rabbit anti-caspase 3 (Bethyl Lab Inc. A303-657A) which recognizes full length protein, while mouse anti-α tubulin monoclonal antibody (1:2000, Sigma, Saint Louis, MO, USA) was used to assess equal amount of protein loaded in each lane.

2.8. Cell proliferation assay

M21 human melanoma cells were seeded on 6-well plates at 5×10^4 cells/well. After 4 h adhesion in complete medium, cells were exposed to compound **4**, sunitinib, and their combination or to compounds **1–3** at 1 μM concentration. After 24 h, 48 h, and 72 h, cell numbers and cell viability were determined using trypan blue exclusion assay. In some experiments, the effect of different treatments on the proliferation of human prostate carcinoma cells (PC3) was determined. Images of growing cultures were taken at different time points.

2.9. Wound healing of M21 human melanoma cells exposed to sunitinib-conjugated compounds

Cell migration was evaluated by an *in vitro* wound healing assay as previously described [41]. M21 human melanoma cells were grown at 80–90% confluence in 35 mm dishes; the cell layer was wounded with a sterile 200 μL pipette tip and tumor cells were grown in the presence of compound **4**, sunitinib, their combination or compounds **1–3**, in standard media for 24 h. The wound was observed after 24 h and photographed using phase contrast microscopy.

2.10. Invasiveness of M21 human melanoma cells exposed to sunitinib-conjugated compounds

Invasiveness of M21 human melanoma cells was determined *in vitro* on Matrigel-precoated polycarbonate filters, with 8 μm pore size, 6.5 mm diameter, 12.5 μg Matrigel/filter, mounted in Boyden's chambers as previously described [41]. M21 human melanoma cells were grown in the presence of compound **4**, sunitinib, their combination or compounds **1–3** in standard media for 24 h. After incubation, 5×10^4 cells (200 μL, in serum-free medium) were seeded in the upper compartment and incubated for 24 h at 37 °C in 10% CO_2 in air. In the lower chamber, complete medium was added as chemoattractant. After incubation, the inserts were removed and the non-invading cells on the upper surface were wiped off mechanically with a cotton swab and the membranes were fixed overnight in ice-cold methanol. Cells on the lower side of the membranes were then stained using the Diff-Quick kit (BD Biosciences) and photographs of randomly chosen fields were taken.

2.11. Xenograft experiments

All experimental procedures involving animals were performed in accordance with the Italian Guidelines and approved by the ethical committee of Animal Welfare Office of Italian Work Ministry. A total of 24 female SCID bg/bg mice aged 6–8 weeks (Charles River Laboratories International, Lecco, Italy) were fed with a regular chow diet (Harlan Laboratories, Indianapolis, US) and water ad libitum. Human melanoma cells were harvested by trypsinization, washed twice in PBS, and then suspended in PBS:Matrigel solution (1:1) at 3.5×10^6 cells per mL; 0.2 mL of cell suspension was injected subcutaneously into the right flank of mice (six animals per group). After 14 days, mice were randomized into treatment groups when tumor volumes reached 120–150 mm^3 and i.p. daily treated with vehicle (PBS), with 10 mg/kg dose of sunitinib malate [42], 20 mg/kg dose of compound **1** or with 40 mg/kg dose of compound **3**, to reach an equimolar concentration of sunitinib. Mice were monitored daily and tumor size was measured every 2 days by a caliper, and tumor volumes were determined by the following formula: volume = (length × width × width)/2. Mice were sacrificed when tumor size in mice treated with vehicle exceeded 600 mm^3, before the occurrence of physical discomfort (rough hair coat, lack of grooming activity, or abnormal posture). Tissues (lung, liver, kidneys, spleen and gastrocnemius muscle) were excised, washed with saline and weighted for successive ethanol extraction, tumors were excised, washed with saline, weighted and separated in halves for ethanol extraction and for histochemical examination by Hematoxylin & Eosin (H&E) staining.

2.12. Biodistribution assessment for sunitinib, compounds *1* and *3*

Tissue samples were homogenized and compounds were extracted with 1 mL of absolute ethanol, following a previously published procedure [28]. Samples were centrifuged (10,000 g, 4 °C, 10 min) and a fixed volume of the supernatant was evaporated to dryness by a gentle nitrogen flux. Pellets were then dissolved in the same volume of HPLC eluent (95% water, 5% MeCN both additioned with 0.1% HCOOH) containing the internal standard (compound **2**), and injected into the HPLC-MS system for quantification. A Thermo Accela U-HPLC system equipped with an Accela Open AS autosampler interfaced to a TSQ Quantum Access Max triple quadrupole mass spectrometer (Thermo, Milan, Italy) with a heated electrospray ionization (H-ESI) ion source was employed for data acquisition. Mass spectrometric analyses were done in positive ion mode. H-ESI interface parameters were set as follows: probe: middle (D) position; capillary temperature: 270 °C; spray voltage: 3.5 kV. Nitrogen was used as nebulizing gas at the following pressure: sheath gas 35 psi; auxiliary gas: 15 arbitrary units (a.u.). Argon was used as the collision gas at a pressure of approximately 1.5 mtorr (1 torr = 133.3 Pa). For quantitative analysis, the following multiple parent ion → product ion transitions were selected: compound **1**: m/z = 480.7 $[M+2H]^{2+} \rightarrow$ m/z = 282.9, 325.7 (tube lens (TL): 95 V; collision energies (CE): 30, 23 eV, respectively); compound **2** (Internal Standard): m/z = 539.8 $[M+2H]^{2+} \rightarrow$ m/z = 282.9, 325.9, 796.4 (TL: 85 V; CE: 28, 23, 22 eV); compound **3**: m/z = 447.9 $[M+3H]^{3+} \rightarrow$ m/z = 121.8, 238.5, 282.6 (TL: 65 V; CE: 42, 45, 22 eV); sunitinib: m/z = 399.3 $[M+H]^{+} \rightarrow$ m/z = 238.1, 283.1, 326.1 (TL: 62 V; CE: 44, 26, 21 eV). A Phenomenex Synergi Fusion C18 column (100 × 2.1 mm; 4 μm particle size) was employed for compound separation following a gradient elution. The flow rate was set at 0.350 mL min^{-1}. Solvent A: water and solvent B: acetonitrile both

additioned of 0.1% v/v formic acid. HPLC gradient was as follows: t (0 min): A: 95%; B: 5%; t(8 min): A: 70%; B: 30%; t(10 min): A: 70%; B: 30%; t(11 min): A: 95%; B: 5% followed by 2 min of column re-conditioning. Retention times were: 6.87 min for **1**, 6.06 min for **2**, 4.87 min for **3**, and 9.17 min for sunitinib. Calibration curves were built for compounds **1**, **3** and sunitinib in the same matrices by spiking stock solutions of compounds in the control tissue extracts. Linearity was assessed in the 1000-1 nM concentration range for sunitinib, 1000-10 nM for **1**; 1000-50 nM for **3**, employing the IS **2** at the final concentration of 100 nM. Correlation coefficient was > 0.99 for all regression lines. Data acquisition and regression analysis were performed by Thermo Xcalibur software v. 2.1 (Thermo, Milan, Italy).

2.13. TUNEL assay for detection of apoptotic cells

To evaluate apoptosis in tumor specimens, we used terminal deoxynucleotidyl transferase (TdT)-mediated dUTP-digoxigenin nick-end labeling (TUNEL assay) technique, to formalin-fixed paraffin-embedded sections, using the commercially available TB235 from Promega. Sections (5–6 μm) mounted on glass slides were deparaffinized, rehydrated through graded alcohols to water, treated with 20 μg/mL proteinase K (37 °C, 10 min at RT) and then washed in PBS and fixed by immersing in 4% methanol-free formaldehyde solution for 5 min at RT. TUNEL assay was then performed according to the instructions by the manufacturer.

2.14. Statistical analysis

Data are shown as mean ± SEM. All experiments were analyzed using Analysis of Variance (ANOVA) test, and differences among the various groups were performed using multiple comparison analysis methods (Tukey tests) using a commercial software (PRISM version 7.0, GraphPad Software Inc., San Diego, CA, USA). $p < 0.05$ was considered significant.

3. Results

3.1. Chemistry and physicochemical characteristics

The three molecular conjugates **1–3** were synthesized by starting from commercial materials in 14 steps and 10–21% overall yields (longest linear sequence), according to a modular mixed in-solution/solid phase synthesis procedure, as previously described [28]. The *in vitro* stability of conjugates **1–3** in 80% v/v rat and human plasma was previously evaluated by HPLC/UV analysis, which showed complete resistance to plasma degradation during the observed time (8 h) [28]. Merging the low molecular weight, lipophilic and permeable sunitinib molecule with the hydrophilic cyclic peptidomimetic c(AmpRGD) via different linkers resulted in “medium-sized” structures **1–3** with new and diversified properties, as shown in Table 1.

Thus, for example, the presence of the pegylated linker (compounds **2** and **3** vs **1**) and the dipeptide presentation (**3** vs **1** and **2**) increased the hydrophilic character, as demonstrated by the increasing negative values of $LogD_{oct,7.4}$ (distribution coefficient in *n*-octanol/buffer at pH 7.4). In addition, the presence of diverse basic sites (i.e. the proline *N*α atom in the AmpRGD within **1–3** and the tertiary amine in the linkers of **2** and **3**) confer different total charge to these molecules, ranging from neutral to highly positive, depending on the structure and/or pH (Table 1; experimental procedure for pKa measurement and related species distribution curves are detailed in the Supporting Information, Fig. S1).

3.2. Inhibition of cell adhesion to the $\alpha_V\beta_3$-integrin ligand vitronectin by conjugates *1 − 3*

In previous works [24,25], the binding affinity of several c(AmpRGD)-based cyclopeptides toward selected integrin receptors was assessed by solid-phase receptor binding assays and, in most cases, these scaffolds showed one-digit nanomolar IC_{50} values toward the $\alpha_V\beta_3$ integrin receptor and appreciable selectivity as confronted to other integrin receptors (Table 2). For example, c(AmpRGD)-NH_2 **4** (used as a reference compound in biological assays in this work), displayed IC_{50} $\alpha_V\beta_3$ 6.1 nM in the competitive displacement of biotinylated vitronectin (VN), a natural ligand of the $\alpha_V\beta_3$ receptor (entry 1). Considering the conjugates **1–3**, their binding competence toward the isolated $\alpha_V\beta_3$ receptor was proven (IC_{50} 1.24–5.1 nM range, entries 2–4), demonstrating that the presence of the sunitinib/linker cargoes did not compromise their good $\alpha_V\beta_3$-integrin targeting capability [28]. In the same study, compounds **1–3** were assayed for their ability to inhibit the adhesion of VN to $\alpha_V\beta_3$-overexpressing endothelial progenitor cells (EPCs), and the results showed that compounds **1** and **3** strongly inhibited cell adhesion (IC_{50} ca. 500 nM) even better than the unconjugated RGD reference (1.8 μM); compound **2**, instead, showed an inferior performance (IC_{50} ca. 10 μM).

In this study, compounds **1–3** were evaluated for their ability to inhibit the adhesion to VN of human melanoma cells (M21), whose abundant $\alpha_V\beta_3$ expression level (95–98%) was evaluated by flow cytometric analysis (see Fig. S2, Supporting Information). Also, for comparison purposes, the unconjugated c(AmpRGD)-NH_2 **4** was challenged, toward both M21 cells and $\alpha_V\beta_3$-lacking cells (namely human prostate carcinoma cells PC3 and human erythroleukemia cells K562), used as negative controls. As shown in Fig. 2 and Table 2, a dose-dependent inhibition on M21 cells was observed for all compounds; in particular, compound **1** exhibited IC_{50} slightly better than that obtained for the unconjugated reference **4**. Similarly, double-RGD-presenting compound **3** showed IC_{50} 5.3 μM, while conjugate **2** inhibited cell adhesion at ca. 20 μM. Thus, the inhibition profile of the adhesion to VN of M21 cells shown by conjugates **1–3** was very similar to that previously observed using endothelial cells. As expected, compound **4** did not inhibit cell adhesion to VN in PC3 and K562 cells.

3.3. Cell internalization of sunitinib and conjugates *1–3*

The cell internalization of sunitinib and the three different conjugates **1–3** was next investigated by using different experimental approaches. Taking advantage of the intrinsic fluorescent emission of the sunitinib moiety, we evaluated the uptake after 1 h and 24 h of free sunitinib at 1 μM concentration and compounds **1–3** (at equimolar sunitinib concentration) on M21 cells by cytofluorimetric assay (Fig. 3A and Fig. S4B). At 24 h we found that sunitinib-associated fluorescence of M21 cells exposed to sunitinib was higher compared to that of M21 cells exposed to compounds **1–3**. Interestingly, the sunitinib-associated fluorescence of M21 cells exposed to compound **3** was higher compared to that of cells treated with compound **1**, while the fluorescence of M21 cells exposed to compound **2** was negligible. The measurements after 1 h incubation revealed that the internalization of conjugates **1–3** was sensibly lower than that of sunitinib, and with a percentage very similar for the three compounds.

To confirm that cell-associated fluorescence was dependent on the cellular internalization of the drug, single cell-associated fluorescence was evaluated using the confocal analysis. M21 cells were examined after 24 h exposure to sunitinib and to the three different compounds **1–3** (1 μM) (see Fig. S4A Supporting Information). We found that the M21 cell population exposed to sunitinib showed a diffused intra-cytoplasmatic green fluorescence signal, corresponding to the internalized sunitinib, while M21 cell population exposed to compounds **1–3** expressed lower fluorescence signals. In particular, a faint signal was revealed after treatment with compound **1**, a negligible signal was revealed after treatment with compound **2**, while treatment with compound **3** determined a more intense fluorescent signal. These results were substantially in line with those obtained with the cytofluorimetric analysis. Further, to investigate the selectivity of cell

Table 1
Selected physico-chemical properties of compounds **1–3** and sunitinib.

cmp	MW (Da)	$LogD_{oct,7.4}$[a]	pKa[b]	Charge of prevailing species (pH 7.4)[c]	Charge of prevailing species (pH 6.0)[c]	tPSA (Å^2)[d]
sunitinib	398.5	2.51	9.08 ± 0.05	+1(98%)	+1(99.9%)	73.23
1	960.0	−2.03	3.92 ± 0.01 6.52 ± 0.01	0(88.4%)	+1(76.3%)	352.64
2	1078.2	−2.56	3.87 ± 0.01 7.25 ± 0.02 8.67 ± 0.01	+1(56.6%)	+2(94.0%)	354.47
3	1788.9	−3.02	3.62 ± 0.02 5.53 ± 0.05 7.08 ± 0.02 8.45 ± 0.01 9.50 ± 0.08	+2(63.6%)	+3(70.3%)	642.35

[a] Distribution coefficient in the n-octanol/buffer system, pH 7.4. Reported are means ± SD.
[b] pKa determined by potentiometric titration at 25 ± 0.5 °C using Sirius T3 instrument. Assays on conpounds 1–3 performed in ionic strength adjusted (ISA) water 0.15 M KCl; sunitinib assays performed in ISA water/co-solvent mixture (MeOH 80% ranging between 38% and 52%). Aqueous pKa determined by Yasuda-Shedlowsky extrapolation.
[c] Determined by distribution curves (see Fig. S1); percentage of the prevailing species in parenthesis.
[d] Total polar surface area as predicted by ACD/Labs (I-Lab 2.0).

Table 2
Cell-free and in-cell adhesion assays of c(AmpRGD)-sunitinib conjugates.

cmp	Isolated Integrin Receptor IC_{50}(nM) ± SD[a]			Cell Adhesion IC_{50}(μM) ± SD[e]			
	$\alpha_v\beta_3$(VN)	$\alpha_v\beta_5$(VN)	$\alpha_5\beta_1$(FN)	EPC(VN)[d] (> 87.5% $\alpha_v\beta_3$; 35–40% $\alpha_5\beta_1$)	M21(VN)[d] (98% $\alpha_v\beta_3$; 10% $\alpha_5\beta_1$; no $\alpha_v\beta_5$)	PC3(VN)[d] (no $\alpha_v\beta_3$; 25% $\alpha_5\beta_1$; 27% $\alpha_v\beta_5$)	K562(VN)[d] (no $\alpha_v\beta_3$; > 85% $\alpha_5\beta_1$ no $\alpha_v\beta_5$)
4	6.1 ± 1.6[b]	315 ± 137[b]	151.6 ± 67.6[c]	1.8 ± 1.3[e]	6.7 ± 1.2	negligible	negligible
1	1.24 ± 0.01[e]		30.7 ± 17.7[e]	0.5 ± 0.7[e]	3.8 ± 1.3		
2	5.1 ± 0.6[e]		101.3 ± 31.3[e]	~10[e]	~20		
3	3.8 ± 0.6[e]		95.8 ± 46.7[e]	0.5 ± 0.6[e]	5.3 ± 0.9		

[a] IC_{50} values were calculated as the concentration of compound required for 50% inhibition of biotinylated VN or FN binding to human, isolated receptors.
[b] Ref [25].
[c] Ref [27].
[d] IC_{50} values were calculated as the concentration of compound required for 50% inhibition of cell adhesion to VN. In parenthesis the percentage of a_Vb_3 integrin expression in EPCs.
[e] Ref [28].

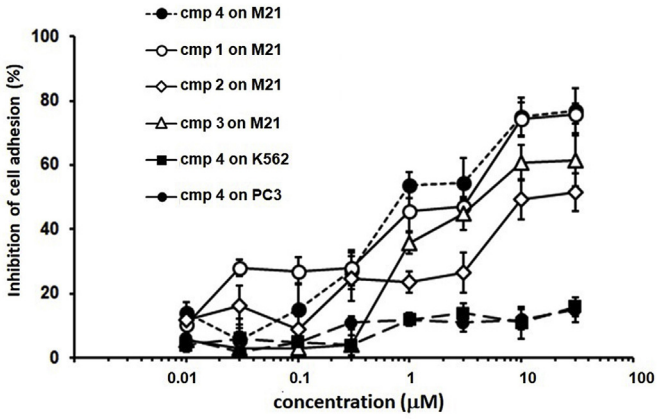

Fig. 2. Inhibition of M21 cell adhesion to VN in the presence of compounds **1–3**, c(AmpRGD)-NH_2 **4**, or sunitinib (2 h). Inhibition of K562 or PC3 cell adhesion to VN in the presence of c(AmpRGD)-NH_2 **4**. The inhibitory activity was calculated as percentage of cell adhesion to VN in untreated cells and was expressed as means ± SEM. Experiments were carried out in triplicate.

internalization, we exposed M21 human melanoma cells, K562 erythroleukemia cells and co-cultures to different treatments using sunitinib, compound **1** or compound **3** for 24 h. As shown in Fig. 3B and C, $\alpha_V\beta_3$-positive and $\alpha_V\beta_3$-negative cells showed strong sunitinib internalization, whereas only a percentage of $\alpha_V\beta_3$-positive cells revealed internalization after the treatment with conjugates **1** and **3**, and, in agreement with the previous results, compound **3** was internalized slightly more efficiently. To confirm the selectivity of cell internalization of these compounds, we carried out an *in vitro* competition experiment. The cells were pretreated for 1 h with 10 μM concentration of c(AmpRGD)-NH_2 **4**, that competes for the integrin binding, and then incubated with compound **3** (1 μM). The dramatically reduced internalization of compound **3** that was registered (Fig. 3D) supports the hypothesis of an integrin-mediated endocytosis of this conjugate. Finally, the late endosomal-lysosomal localization of sunitinib and conjugates **1–3** was evaluated using the anti-Rab7 antibody. As shown in Fig. 3E, untreated cells showed no signal from Rab7 protein, as expected in cells not subjected to any endocytic stimulation, while only free sunitinib colocalizes with Rab7. Compounds **1** and **3** (green fluorescence signal) were dispersed throughout the cytoplasm and showed a reduced signal from the Rab7 antibody (red fluorescence signal) and also a negligible colocalization (orange fluorescence signal) with Rab7 protein.

*3.4. Effects of sunitinib and conjugates **1–3** on ERK1/2 phosphorylation, invasive phenotype, and proliferation*

To evaluate the effect of the different compounds on the cell signaling, we tested ERK1/2 inhibition of phosphorylation in M21 cells exposed to either compounds **1–3**, free sunitinib or c(AmpRGD)-NH_2 **4** (1 μM) for 1 h (Fig. 4A). It was found that the use of 1 μM sunitinib, alone or in combination with **4**, completely inhibited ERK1/2 phosphorylation, while the use of **4** alone had a minimal effect. Treatment

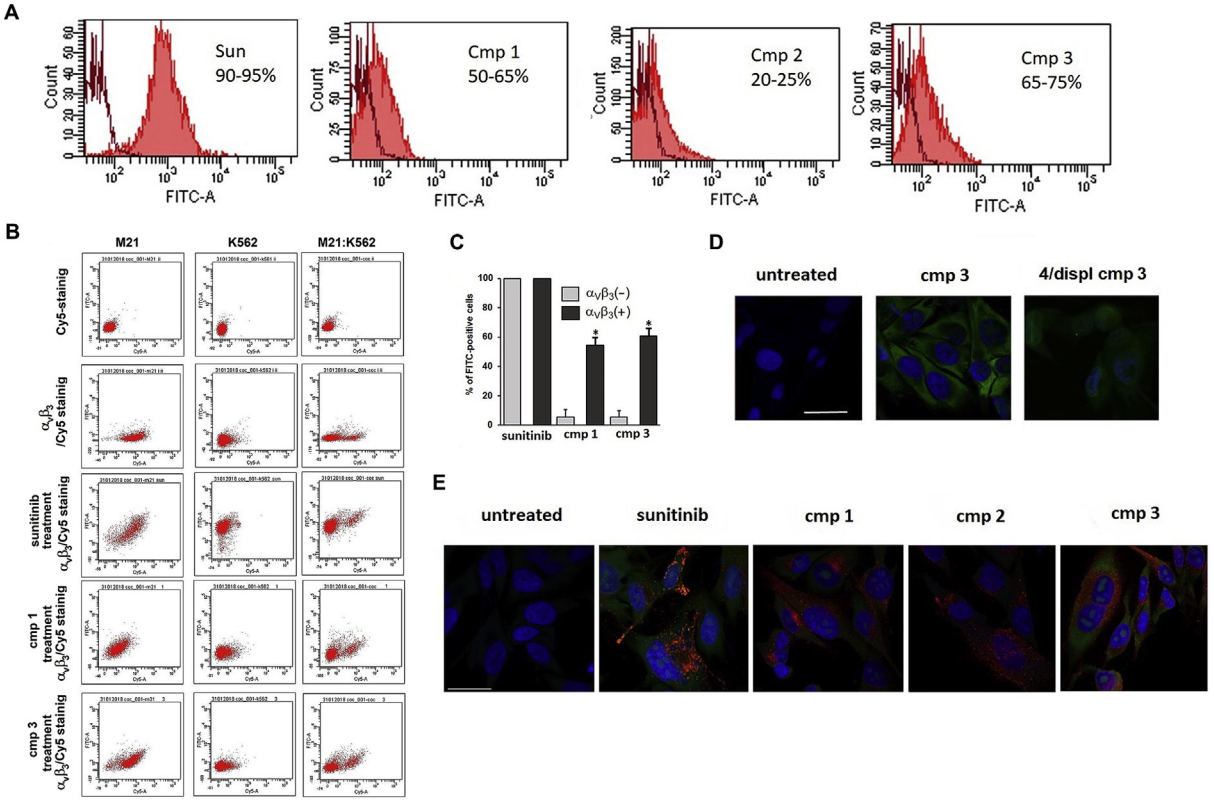

Fig. 3. A) Representative images of internalization of conjugates **1–3** or sunitinib as assessed by flow cytometry measurements. Fluorescence intensity (FacScan FLT1/FITC-A) in M21 cells treated for 24 h with sunitinib or conjugates **1–3** at 1 μM. Percentage intervals indicate fluorescence(FITC-A)-positive cells from three independent experiments. B) Scatterogram of $\alpha_V\beta_3$ staining (Cy5-A) and sunitinib (FITC-A) associated green fluorescence of M21 cells, K562 cells and M21:K562 cell co-cultures upon treatment with sunitinib or conjugated compounds (1 μM) for 24 h. C) Quantification of sunitinib-associated green fluorescence using flow-cytometry analysis of M21:K562 cell co-cultures treated with sunitinib or conjugated compounds (1 μM) for 24 h. Each column represents the mean values ± SEM of three experiments (*$p < 0.01$) in M21 vs K562 cells. D) Representative images of fluorescence confocal analysis of M21 untreated, or exposed to compound **3** at 1 μM for 3 h or to compound **4** at 10 μM for 1 h before exposure to compound **3** for 3 h. After incubation, cells were fixed and processed for fluorescence confocal imaging. The cell nuclei were stained with DAPI. Scale bar, 20 μm. Experiments were performed at least three times. E) Immunofluorescence analysis of M21 cells exposed for 24 h to different compounds: anti-Rab7 (red); sunitinib and cAmpRGD-sunitinib conjugates (green). The nuclei were stained with DAPI (blue). Scale bar, 20 μm. (For interpretation of the references to colour in this figure legend, the reader is referred to the Web version of this article.)

with the three conjugates **1–3** at the same concentration strongly reduced ERK1/2 phosphorylation, even if to a lower extent than sunitinib, with compound **3** inhibiting ERK1/2 phosphorylation better than compounds **1** and **2**. We also found that the treatment with compounds **1–3** compromised M21 cells migratory ability and invasiveness. In particular, the treatment with compounds **1–3** reduced the ability of M21 cells to close the wound, better than after the treatment with sunitinib, and in a similar way to that obtained after the treatment with the combination of c(AmpRGD)-NH_2 **4** and sunitinib (Fig. 4B). In addition, compounds **1–3** significantly reduced M21 invasiveness through matrigel-coated filters (Fig. 4C).

To further investigate the role of the different compounds on cell proliferation, we evaluated M21 growth during 72 h exposure to 1 μM daily treatments of the different compounds (Fig. 4D). We found that after 48 h, inhibition of cell proliferation was significantly reduced in cells exposed to the treatment with conjugates **1–3**, c(AmpRGD)-NH_2 **4**, sunitinib alone or in combination with **4**, as compared to untreated cells. In addition, after 48 h, a certain synergistic inhibitory effect was observed for the combination treatment, which was annihilated after 72 h. Interestingly, after 72 h, compound **3** was able to significantly inhibit M21 cells proliferation more efficiently than the combination treatment and slightly less efficiently than free sunitinib. The inhibition of growth obtained using the other two conjugates **1** and **2** was comparable to that of the combination treatment. Interestingly, we found that the different treatments induced no cytotoxic effect on M21 viability, evaluated using the trypan blue exclusion assay and cell cycle analysis (data not shown). To better understand the effect of the compounds on M21 cells growth, we evaluated the levels of caspase 3 activation after 72 h exposure to the conjugates **1–3**, c(AmpRGD)-NH_2 **4**, sunitinib alone or in combination with **4.** We found that the exposure to compound **1** and **3** induced the reduction of the entire form of caspase 3 (Fig. S6). Interestingly, as a negative control, $\alpha_V\beta_3$-integrin negative PC3 cells exposed to the same treatments revealed a strong inhibition on cell proliferation only using sunitinib, independently if used alone or in combination with c(AmpRGD)-NH_2 **4** (data shown as images from growing cultures, upper panel in Fig. 4D).

Next, M21 cells were exposed to the various compounds, at 1 μM concentration, every other day for 6 days in order to verify the possible escape from drug efficacy. After this treatment, M21 cells were washed and seeded at low density and allowed to grow for additional 14 days, using the same treatment schedule. M21 cell clonogenic activity was determined, by the use of the colony forming assay and expressed as surviving factor SF. Interestingly, we found that the treatment with c(AmpRGD)-NH_2 **4**, compound **1** and compound **3**, significantly reduced M21 cell clonogenic activity expressed as SF. Surprisingly, a prolonged treatment with sunitinib (and also compound **2**) significantly increased M21 cell proliferation, showing a SF in a range of 3 ± 0.5, indicating a promotion of escaping mechanisms in sunitinib-treated cells but not in cells treated with compound **3** (Fig. 5A).

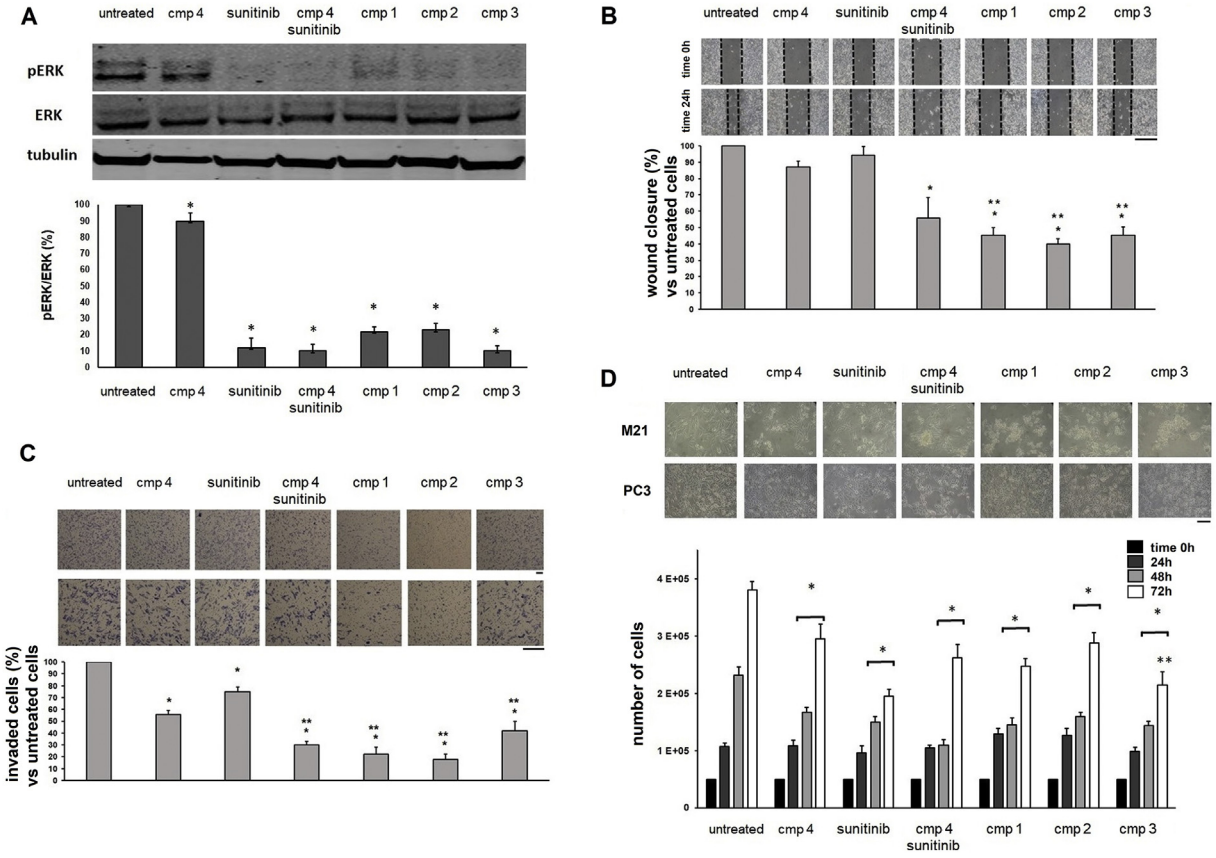

Fig. 4. A) Expression of phosphorylated and total ERK and tubulin in M21 cells exposed to compounds **1–3**, c(AmpRGD)-NH_2 **4**, or sunitinib for 1 h (1 μM). Upper panels are representative immunoblots and the lower panels are mean densitometric values ± SEM from three independent experiments of phosphorylated proteins normalized to their respective total protein. *p < 0.05 in comparison with untreated by ANOVA followed by Newman-Keuls test. B) Upper panels, representative images of the wound healing assay of M21 melanoma cells grown in the presence of compound **4**, sunitinib, their combination or compounds **1–3**. Images are taken immediately after scratching (time 0) and 24 h later (time 24). Scale bar, 1 mm. Lower panels, quantification of wound healing closure. Data are percentages of wound closure compared to closure in untreated cells and are expressed as mean value ± SEM of at least three independent experiments. *p < 0.05 vs untreated; **p < 0.05 vs sunitinib. C) Upper panels, representative images of invasiveness of M21 melanoma were grown in the presence of compound **4**, sunitinib, their combination or compounds **1–3** in standard media for 24 h allowed to migrate toward Matrigel-coated filters. Scale bar, 1 mm. Lower panel, quantification of invasiveness. Data are percentages of migrated cells compared to untreated cells and expressed as mean value ± SEM of at least three independent experiments. *p < 0.05 vs untreated, **p < 0.05 vs sunitinib. D) Cell proliferation of M21 cells exposed once to compounds **1–3**, c(AmpRGD)-NH_2 **4**, or sunitinib for 24 h, 48 h, and 72 h (1 μM). Upper panel: representative images of M21 cells and PC3 cells exposed once to compounds **1–3**, c(AmpRGD)-NH_2 **4**, or sunitinib for 72 h. Lower panel: Histogram showing the number of living cells (mean value ± SEM) of three independent experiments. *p < 0.05 in comparison with untreated 48 h and 72 h respectively, **p < 0.05 in comparison with combinatorial treatment.

*3.5. In vivo effect of sunitinib, conjugates **1** and **3** on targeted delivery xenografts and biodistribution studies*

Scid beige mice were s.c. injected with 0.7×10^6 cells in a PBS:Matrigel 1:1 solution. One week after the injection, when the s.c. tumors were palpable, mice were randomized into 4 different groups comprising the control group (treated with PBS), and the groups treated with sunitinib malate, compound **1** or compound **3**. The daily dose of sunitinib malate was 10 mg/kg, while the dose of **1** (20 mg/kg) and **3** (40 mg/kg) was calculated to have the equimolar concentration of sunitinib. Drugs were i.p. administered [40] every day and tumor growth was measured by the use of a caliper every other day. Mice of each treatment group did not show any sign of discomfort or weight loss during the 2-weeks observation time, even though the evaluation of cardiotoxic and hepato/nephrotoxic effect in treated mice was not carried out. Compared to untreated mice, tumor growth of mice treated with sunitinib malate was significantly reduced, reaching almost 22% reduction in tumor weight at the end of the treatment (Fig. 5B), and a similar reduction was obtained using conjugate **1**. Very interestingly, treatment with compound **3** reduced the growth of tumors with greater efficacy, as compared to both untreated mice (55% reduction in tumor weight), and those treated with sunitinib (Fig. 5B). Histological examination showed high cellularity in tumor tissues of untreated mice. Tumor cells are cohesive showing cellular overlap and little pleomorphism. Signs of necrosis are present near the periphery of the lesion, and large and vascular lacunas can be appreciated throughout the lesion. Tumor tissue sections of mice treated with sunitinib showed a reduced cellular staining, reduced vascular lacunas and signs of cellular damages, highlighted by the swelling of tumor cells that is revealed by their light stained large cytoplasm and giant nuclei with chromatin clumping. Cellular damages are more pronounced in the tumors of mice treated with the RGD-sunitinib conjugates. In particular, tumors treated with compound **3** showed a high degree of hydropic degeneration, while sporadic signs of tissue necrosis were present within the lesion (Fig. 5C). In addition to that we evaluated the presence of signs of intratumoral apoptosis using the TUNEL assay. We observed that the tumor lesions of mice treated with compound **1** or compound **3** exhibited an enhanced apoptosis, compared with the tumor lesions of untreated mice and mice treated with sunitinib (Fig. S7).

Finally, we evaluated whether the amount of sunitinib, compounds **1** and **3** in the tumor and in different tissues of the treated mice might represent a possible driver of compound **3** better efficacy (Fig. 5D). The

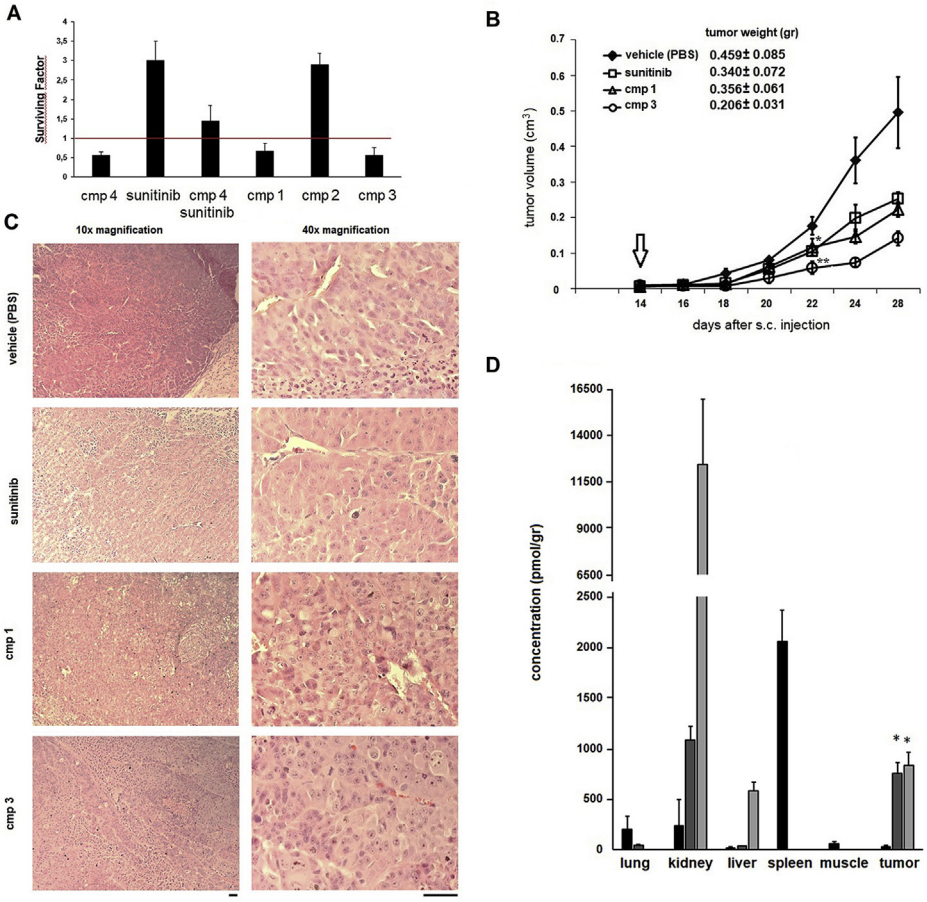

Fig. 5. A) Inhibition of M21 cell proliferation. M21 cells were grown in the presence of compounds **1–3**, **4**, or sunitinib (for 6 days). After the incubation cells were seeded at low density and colonies were allowed to grow for 2 weeks in standard medium and treated with compounds **1–3**, **4**, or sunitinib every other day. The surviving factor (SF) was calculated (number of clones from treated cells)/(treated cells seeded × Cloning Efficiency). The assay was carried out in triplicate, and the mean values ± SEM are shown. Three independent experiments were performed and representative results from one experiment were shown. B) Tumor growth curves and tumor weight change (mean ± SEM in grams) at the end of treatment of tumor bearing mice, i.p. injected daily with vehicle, sunitinib or compounds **1** or **3**. Arrow indicates the start of the treatment. Data are expressed as mean value ± SEM from 6 mice. *p < 0.005 vs vehicle and **p < 0.005 vs sunitinib. C) Representative images of tumor tissue sections of excided in H&E staining (10X and 40X magnification). Scale bar, 50 μm. D) Evaluation of concentration at 24 h after the last treatment in different tissues excided from mice treated with sunitinib (black columns), compound **1** (dark grey columns) or compound **3** (light grey columns). Data represent the mean value ± SEM of drug concentration. *p < 0.005 vs sunitinib.

mice were sacrificed 24 h after the last i.p. administration. The concentration of compounds **1** and **3** in the tumor lesions was significantly higher than that of sunitinib. Sunitinib distributed in several tissues, in fact, we found that sunitinib was still present in the lungs, muscles and above all in the spleen at a higher concentration than compounds **1** or **3**. However, compounds **1** and **3** were found at a higher concentration than sunitinib in the excretory organs, like kidneys and liver. These results account for the prolonged circulation time of compound **3** compared to compound **1** and sunitinib, and for a selective tissue specificity and a lower off-organ distribution.

4. Discussion

Advanced melanoma has long been one of the incurable malignant cancers since the advent of targeted therapy and immune checkpoint inhibitors. Despite the clinical advantages deriving from the use of those therapeutic treatments, the insurgence of drug resistance and the development of severe and life-threatening adverse effects may cause discontinuation of therapeutic treatment. Hence, the progression-free survival and overall survival of metastatic melanoma patients remain critical.

The focus of this work was placed upon three molecular conjugates, compounds **1–3** (Fig. 1), which are originated by the covalent connection of two “active modules” namely, the known anti-angiogenic and antitumor sunitinib moiety and the $\alpha_V\beta_3$-integrin antagonist c (AmpRGD).

Integrin receptor $\alpha_V\beta_3$ represents an eligible target for the selective discrimination of cancer cells due to its overexpression in advanced melanoma cells and its recognized role in metastatic disease progression [29,43–45]. The molecular basis for the use of sunitinib in this preclinical model of advanced melanoma resides in the following observations. Sunitinib is an antitumor and anti-angiogenic multi-kinase inhibitor, which exerts its activities on diverse tyrosine kinase-associated receptors (RTK) of different growth factors, such as Vascular Endothelial Growth Factor Receptors 1–3 (VEGFR-1, -2, and -3), Platelet-Derived Growth Factor Receptors alpha and beta (PDGFRα and PDGFRβ), Fms-like tyrosine kinase-3 (Flt-3), c-KIT and Colony Stimulator Factor-1 Receptor (CSFR-1), whose downstream pathways often match and combine with melanoma-BRAF-MEK1/2 pathway (Fig. 6). Sunitinib is clinically approved for the treatment of metastatic renal cell carcinoma (RCC), imatinib-resistant gastrointestinal stromal tumors (GISTs), and metastatic pancreatic neuroendocrine tumors [30–33]. It has been observed that, in patients with advanced melanoma, increased tumor microvascular density and high level of soluble angiogenic factors (bFGF-2, VEGF, and IL-8) correlate with worse prognosis and reduced progression-free survival [46,47]. Furthermore, VEGF has been demonstrated to play a role in the pathogenesis, growth, and metastatic progression of melanoma [48]. Anti-angiogenic agents, including sunitinib, have shown some clinical efficacy in the treatment of melanoma, with combination therapies (e.g. association with stereotactic body radiation therapy or therapeutic vaccine) being the most promising, though problems associated with real long-term effectiveness, resistance mechanisms insurgence and dosage-dependent toxicity still hamper their use [32,49–52]. Finally, it has been recently shown that sunitinib possesses interesting immune enhancer features, thus justifying the opportunity to explore its use in the field of metastatic melanoma [53–55].

Some sunitinib analogue conjugates have been synthesized and evaluated as either lysozyme-based targeting agents [56,57], imaging tools [58], or GnRH-receptor directed agents [59], but no covalent and

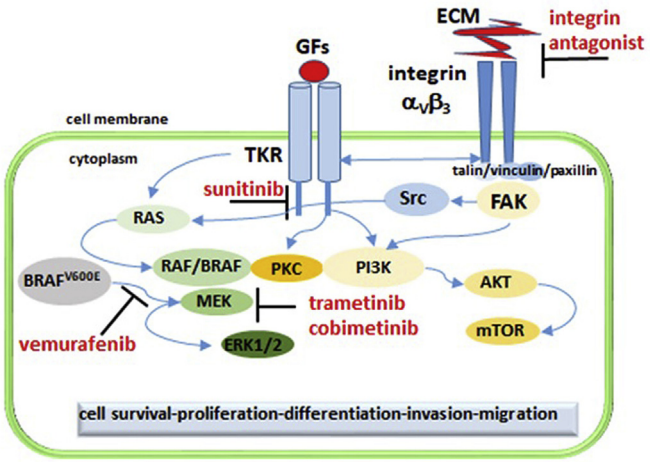

Fig. 6. Receptor-mediated signaling in $\alpha_V\beta_3$-overexpressing melanoma cells. Activation of cell-surface receptors such as $\alpha_V\beta_3$ integrin and other tyrosine kinase growth factor receptors leads to the activation of the RAS/ERK, PI3K/AKT pathways. The actions of small molecule intracellular antagonists sunitinib, extracellular integrin antagonist and those of targeted therapeutic drugs (vemurafenib, dabrafenib and tramentinib i.e.) are shown. ECM, extracellular matrix; GR, growth factor; TKR, tyrosine kinase receptor (VEGFR1-3 Vascular Endothelial growth factor, cKIT/CD117, or PDGFR Platelet derived growth factor); FAK, focal adhesion kinase; ERK, extracellular signal-regulated kinases.

robust conjugation to a $\alpha_V\beta_3$-integrin directed ligands has been reported [28].

In this work, the chemical robustness of compounds **1–3** featuring uncleavable linkers anticipated that both the observed physicochemical properties (i.e. hydrophilic/lipophilic balance, total charge, solubility, Table 1), and the subsequent functional behavior in a biological environment (i.e cell-targeting ability, cell uptake, anti-tumor efficacy) are associated to these conjugates as intact, unique chemotypes, and not to their individual, separated components.

Cell adhesion assays performed on both $\alpha_V\beta_3$-positive M21 cells and $\alpha_V\beta_3$-negative PC3 and K562 cells demonstrated that conjugates **1–3** (as well as unconjugated compound **4**) are good antagonists of M21 melanoma cells adhesion to the natural ligand vitronectin. Though the involvement of other adhesive receptors cannot be completely ruled out (e.g integrin receptors other than $\alpha_V\beta_3$), the results in Table 2 and Fig. 2 support the notion that the very good and quite selective binding affinity of the AmpRGD portion toward the $\alpha_V\beta_3$ receptor is mainly responsible for the binding competence of these conjugates towards M21 cells. It is important to highlight that the observation time of the inhibition of adhesion assay is 2 h-long; thus, even high doses of the sunitinib portion within conjugates **1–3** are not able to affect the cell viability, pointing to the conclusion that inhibition of cell adhesion only relies on RGD antagonism.

Since one of the main interests in therapeutic combination treatments is lowering the dosage of the single drugs, overcoming drug resistance [60], we chose to perform the subsequent experiments using the 1 μM concentration, which may allow us to highlight possible synergistic effects. Indeed, the suboptimal reduction of SF (0.8 ± 0.05) after the treatment with sunitinib malate at 1 μM concentration was similar to that obtained after the treatment with the combination of sunitinib and c(AmpRGD)-NH_2 **4** (Fig. S3).

As mentioned before, the different molecular and physicochemical properties of the conjugates **1–3** with respect to sunitinib may heavily affect their cellular internalization. Cytofluorimetric analysis was exploited to study the internalization, taking advantage from the fluorescence properties of sunitinib. After a 24 h exposition, the compounds **1–3** were less internalized than sunitinib in M21 cells. However, we found that, among the three conjugates, compound **3** enters cells more easily than compound **1**, in turn better internalized than compound **2**, following a trend similar to that observed for the cell binding affinities of these compounds. A series of different experiments namely, i) uptake measurements by cytofluorimetry on $\alpha_V\beta_3$-positive M21 cells (Fig. 3A), ii) uptake using co-cultures of $\alpha_V\beta_3$-positive M21 cells and $\alpha_V\beta_3$-negative K562 (Fig. 3B and C), and iii) uptake of compound **3** on M21 pretreated with excess RGD ligand **4** (Fig. 3D), concurred to emphasize the role of integrin $\alpha_V\beta_3$ in mediating the selective uptake of compounds **1–3** in M21 cells, as compared to the unselective uptake of free sunitinib.

To further define possible different behavior in the distribution of sunitinib and conjugates **1–3** at the subcellular level, the anti-Rab7 antibody was used (Fig. 3E). Sunitinib co-localizes with Rab7 protein, confirming its preferential accumulation in late endosomal and lysosomal vesicles; in fact, sequestration of sunitinib within lysosomal compartments was reported as a mechanism of tumor resistance to sunitinib therapy both *in vitro* and *in vivo* [61–63]. Conjugates **1–3**, instead, seem to be freely distributed in the cytoplasm.

Though the actual reasons for the absence of lysosomal accumulation of compounds **1–3** are still obscure, it could be conceivable that in the case of these novel conjugates, whose characteristics as medium-size, hydrophilic and multiple basic sites-bearing molecules have been discussed (Table 1) a receptor-mediated internalization process could be invoked. Once internalized in the acidic subcellular compartments as endosomes, multiple charged species prevail (Table 1), which could be responsible for endosomal escape via the known proton sponge effect, with subsequent dispersion into the cytoplasm [64]. Moreover, we found out that compounds **1** and **3** can trigger the activation of an apoptotic program that is not triggered by sunitinib (Fig. S6). Based on these two observations, compounds **1–3** could represent a viable "alternative" to sunitinib to escape the insurgence of resistance mechanisms upon anti-angiogenic and/or anti-tumor treatments.

To evaluate the therapeutic efficacy of conjugates **1–3** at the molecular level, and considering that possible primary targets of the TKI sunitinib portion are multiple and closely intertwined pathways might be triggered (vide supra, Fig. 6), we reasoned that evaluation of p-ERK1/2 inhibition would be a rational first choice as read-out of their intracellular activity.

It was found that ERK1/2 phosphorylation was completely abolished by 1 h treatment with 1 μM sunitinib malate and partially, but still efficiently, reduced by the treatment with three conjugates **1–3** (Fig. 4A), while compound **4** was less efficient. The similar behavior exerted by the compounds **1–3** in inhibiting ERK1/2 phosphorylation at 1 h is in line with the observation of similar amounts of the three conjugates being internalized in M21 cells after 1 h incubation (Fig. S4B), even if we cannot exclude that the antagonistic effect of the RGD portion on integrin $\alpha_V\beta_3$ can contribute to the inhibition of MAPK pathway (Fig. 6).

Therefore, we investigated the effect of the different treatments at the biological level, and we evaluated whether these compounds may affect melanoma cells motility and invasiveness (Fig. 4C and D). We found a significant reduction in both cell motility and invasive ability after 24 h treatment with compounds **1–3** (1 μM) as compared to untreated cells. Interestingly, M21 cells motility and invasiveness potential were slightly affected by sunitinib at the same concentration, while the combination of c(AmpRGD)-NH_2 **4** and sunitinib resulted in a synergic activity in the inhibition of motility and invasiveness, though to a lesser extent than the covalent conjugates. This behavior seems to emphasize the superior role of the covalent conjugation of the two active units as compared to the individual combined components. Migration and invasion require cell attachment to extracellular proteins mediated by integrins and other adhesion molecules, and their inhibition is therefore mainly performed by the RGD portion of the compounds **1–3**, that exert their function mostly at the extracellular level. In fact, compound **2**, which is internalized at a lesser extent than **1** and **3** in the 24 h period, resulted to be more active. In addition, to support

the antagonist effect of the conjugates, we investigated the action of compounds **1–3** and AmpRGD-NH_2 **4** on cytoskeletal reorganization in firmly adherent M21 cells. We found that 1 h treatment with 1 μM conjugates **1–3** causes significant cytoskeletal disorganization (Fig. S5). This result demonstrates not only that the conjugated compounds are able to engage the integrin receptors in adherent cells, but also that their effect (at 1 μM concentration) is more powerful than that of AmpRGD-NH_2 **4**, in line with the wound healing and invasiveness assays.

Having in mind the importance of the issue of dosage reduction, we explored the anti-proliferative effect on melanoma cells using a low-concentration, prolonged drug treatment rather than a high-concentration, brief treatment (Fig. 4D). We found that low concentrations (1 μM) of the three conjugates **1–3** significantly reduced the growth of M21 melanoma cells at 48 h and 72 h compared to untreated cells; in addition, we found that only compound **3** strongly reduced melanoma cells growth with comparable efficacy as sunitinib and more effectively than the combination treatment. Once again, this assessed the superiority of the covalent conjugation of the two active modules within **3** over their simple combination. While no acute cytotoxic effect was found after the treatment, neither any cell cycle arrest was observed, a possible explanation of the effect of conjugated compounds on cell proliferation might come from the evaluation of caspase 3 activation. We found that compounds **1** and **3** induced the reduction of the entire form of caspase 3. Thus, the induction of apoptosis might explain the reduction of proliferation after the treatment with the conjugated compounds. It is important to note that melanoma cell morphology was deeply changed after treatment with conjugates **1–3,** whereas PC3 cells morphology and proliferation (Fig. 4D upper panel) were not affected, confirming that inhibition of melanoma cell proliferation is mediated, also, by $\alpha_V\beta_3$ integrin recognition.

To investigate the effect of a chronic treatment, the clonogenic activity of cells exposed to different treatment was evaluated, and surprisingly we found a significant reduction in M21 SF after treatment with c(AmpRGD)-NH_2 **4**, similar to that obtained by the treatment with compound **1**, or **3**. The treatment with sunitinib, on the other hand, determined a significant increase in SF, probably due to the instauration of resistance mechanisms in treated cells. In addition, the combination of c(AmpRGD)-NH_2 **4** and sunitinib revealed a SF lower than that of cells treated with sunitinib malate alone (Fig. 5A).

Finally, to evaluate the effect of the conjugated compounds *in vivo*, we treated melanoma tumor-bearing mice with a sub-optimal dose of sunitinib alone in comparison with compounds **1** and **3** (Fig. 5B). We opted to use 4-fold decreased dosage (ca. 10 mg/kg/d sunitinib equivalent) [28,42] to better emphasize possible differences between the tested compounds and evaluate the impact of the *in vivo* treatment using low-toxicity dosage. Tumor growth was significantly reduced in mice treated with either sunitinib alone, compound **1**, or compound **3**, as compared to untreated mice. In particular, while the behavior of sunitinib-treated mice was similar to that observed for mice treated with conjugate **1**, the growth of tumor in mice treated with compound **3** was significantly reduced also compared to sunitinib treatment. Furthermore, in a preliminary, yet incomplete biodistribution assessment (Fig. 5D), we found that conjugates **1** and **3** were selectively localized (24 h after the last i.p. injection) in $\alpha_V\beta_3$-expressing neoplastic lesions and in the excretory organs, whereas sunitinib was found in every other analyzed tissue. These very preliminary results confirm the unspecificity of sunitinib distribution [65] and underline the selective tumor-targeting ability of the conjugated compounds **1** and **3** as robust and intelligent sunitinib-targeting vehicles *in vivo*. The reduction in tumor growth might partially depend on the cellular hydropic degeneration constantly sustained by the treatment with compound **3**, causing a chronic tissue damage and the subsequent activation of apoptosis (Fig. S7). Despite compounds **1** and **3** were found in the same amount in the lesion, the more efficient effect of compound **3** on tumor growth might be attributed to the presence of the two c(AmpRGD) moieties responsible of a better cellular internalization than compound **1**.

5. Conclusions

The molecular conjugates **1–3** derived from the robust, covalent connection of well-established active components namely, sunitinib and c(AmpRGD) active units, resulted in interesting tools to investigate the metastatic melanoma disease. In particular, compound **1** and, even better, compound **3**, drastically reduced the growth of melanoma xenografts on tumor-bearing mice compared to free sunitinib at low doses, and selectively localized in the tumor tissue.

The selective uptake of these conjugates by melanoma cells was mainly due to the recognition and binding ability to the $\alpha_V\beta_3$-integrin, which is overexpressed in the melanoma cells used in this study; the observed *in vitro* and *in vivo* melanoma cell-selectivity is a good premise for targeted therapy with consequent dosage reduction and, hopefully, decreased adverse and toxic effects on healthy tissues, aspects that need a future investigation.

The molecular conjugates **1–3** have physicochemical properties different from the constituting units, which consequently dictate a biological behavior (both *in vitro* and *in vivo*) different from the small-molecule sunitinib. In particular, a decreased aggressiveness in the M21 cell population was observed under chronic treatment with conjugates **1** and **3** as compared to sunitinib. Also, the localization of conjugates **1–3** in the cytosol as opposed to the compartmentalization of sunitinib in lysosomes of M21 cells suggests possible overcoming of another resistance mechanism involving the sunitinib drug.

Due to the multiple biological targets of the sunitinib, it is hard to strictly define all the targets of conjugates **1–3**; however, their action as antagonists of the $\alpha_V\beta_3$-integrin and MAPK inhibitors, open the way for the use of these selective conjugates as drugs able to counteract the compensatory escape mechanisms that tumor cells establish against conventional pharmacological treatments.

Author contributions

The manuscript was written through the contributions of all authors. All authors have given approval to the final version of the manuscript.

Conflicts of interest

None.

Acknowledgments

This work was supported by Ente Cassa di Risparmio di Firenze (Protocol Number 2013.0688), by Ministero dell'Istruzione, dell'Università e della Ricerca (MIUR, PRIN2015 prot.20157WW5EH (5 February 2017/2020)) and by the Istituto Toscano Tumori (Grant Number 7197 29/12/2009).

Appendix A. Supplementary data

Supplementary data to this article can be found online at https://doi.org/10.1016/j.canlet.2018.12.021.

References

[1] SEER Stat Fact Sheets: Melanoma of the Skin. National Cancer Institute; Surveillance, Epidemiology, and End Results Program Website. http://seer.cancer.gov/statfacts/html/melan.html [National Cancer Institute. Surveillance, Epidemiology and End Results. http://www.seer.cancer.gov/statfacts/.

[2] A.M. Eggermont, A. Spatz, C. Robert, Cutaneous melanoma, Lancet 383 (2014) 816–827, https://doi.org/10.1016/S0140-6736(13)60802-8.

[3] A. Vecchiato, E. Zonta, L. Campana, G. Dal Bello, M. Rastrelli, C.R. Rossi,

M. Alaibac, Long term survival of patients with invasive ultra-thin cutaneous melanoma: a single-center retrospective analysis, Medicine (Baltim.) 95 (2016 Jan) e2452, https://doi.org/10.1097/MD0000000000002452.
[4] C. Garbe, K. Peris, A. Hauschild, P. Saiag, M. Middelton, L. Basthold, J.J. Grob, J. Malvehy, J. Newton-Bishop, A.J. Stratigos, H. Pehamberger, A.M. Eggermont, European dermatology forum (EDF), European association of dermato-Oncology (EADO), European Organization for research and treatment of cancer (EORTC) diagnosis and treatment of melanoma. European consensus-based interdisciplinary guideline- update 2016, Eur. J. Cancer 63 (2016) 201–217, https://doi.org/10.1016/j.ejca.2016.05.005.
[5] N.J. Ives, S. Suciu, A.M.M. Eggermont, J. Kirkwood, P. Lorigan, S.N. Markovic, C. Garbe C, K. Wheatley, International Melanoma Meta-Analysis Collaborative Group (IMMCG). Adjuvant interferon-α for the treatment of high-risk melanoma: an individual patient data meta-analysis, Eur. J. Cancer 82 (2017) 171–183, https://doi.org/10.1016/j.ejca.2017.06.006.
[6] J.E. Gershenwald, R.A. Scolyer, K.R. Hess, V.K. Sondak, G.V. Long, M.I. Ross, A.J. Lazar, M.B. Faries, J.M. Kirkwood, G.A. McArthur, L.E. Haydu, A.M.M. Eggermont, K.T. Flaherty, C.M. Balch, J.F. Thompson, For members of the American Joint committee on cancer melanoma Expert panel and the International melanoma database and discovery Platform. Melanoma staging: Evidence-based changes in the American Joint committee on cancer eighth edition cancer staging manual, Ca - Cancer J. Clin. 67 (2017) 472–492, https://doi.org/10.3322/caac.21409.
[7] J.J. Luke, G.K. Schwartz, Chemotherapy in the management of advanced cutaneous malignant melanoma, Clin. Dermatol. 31 (2013) 290–297, https://doi.org/10.1016/j.clindermatol.2012.08.016.
[8] M.B. Atkins, M.T. Lotze, J.P. Dutcher, R.I. Fisher, G. Weiss, K. Margolin, J. Abrams, M. Sznol, D. Parkinson, M. Hawkins, C. Paradise, L. Kunkel, S.A. Rosenberg, High-dose recombinant interleukin 2 therapy for patients with metastatic melanoma: analysis of 270 patients treated between 1985 and 1993, J. Clin. Oncol. 17 (1999) 2105–2116, https://doi.org/10.1200/JCO.1999.17.7.2105.
[9] J.J. Luke, K.T. Flaherty, A. Ribas, G.V. Long, Targeted agents and immunotherapies: optimizing outcomes in melanoma, Nat. Rev. Clin. Oncol. 14 (2017) 463–482, https://doi.org/10.1038/nrclinonc.2017.43.
[10] T. McKibbin, Melanoma: understanding relevant molecular pathways as well as available and emerging therapies, Am. J. Manag. Care 21 (2015) S224–S233 PMID: 26619296.
[11] P.B. Chapman, A. Hauschild, C. Robert, J.B. Haanen, P. Ascierto, J. Larkin, R. Dummer, C. Garbe, A. Testori, M. Maio, D. Hogg, P. Lorigan, C. Lebbe, T. Jouary, D. Schadendorf, A. Ribas, S.J. O'Day, J.A. Sosman, J.M. Kirkwood, A.M. Eggermont, B. Dreno, K. Nolop, J. Li, B. Nelson, J. Hou, R.J. Lee, K.T. Flaherty, G.A. McArthur, BRIM-3 Study Group. Improved survival with vemurafenib in melanoma with BRAF V600E mutation, N. Engl. J. Med. 364 (2011) 2507–2516, https://doi.org/10.1056/NEJMoa1103782.
[12] R. Fisher, J. Larkin, Vemurafenib: a new treatment for BRAF-V600 mutated advanced melanoma, Cancer Manag. Res. 4 (2012) 243–252, https://doi.org/10.2147/CMAR.S25284.
[13] G. Bollag, P. Hirth, J. Tsai, J. Zhang, P.N. Ibrahim, H. Cho, W. Spevak, C. Zhang, Y. Zhang, G. Habets, E.A. Burton, B. Wong, G. Tsang, B.L. West, B. Powell, R. Shellooe, A. Marimuthu, H. Nguyen, K.Y. Zhang, D.R. Artis, J. Schlessinger, F. Su, B. Higgins, R. Iyer, K. D'Andrea, A. Koehler, M. Stumm, P.S. Lin, R.J. Lee, J. Grippo, I. Puzanov, K.B. Kim, A. Ribas, G.A. McArthur, J.A. Sosman, P.B. Chapman, K.T. Flaherty, X. Xu, K.L. Nathanson, K. Nolop, Clinical efficacy of a RAF inhibitor needs broad target blockade in BRAF-mutant melanoma, Nature 467 (2010) 596–599, https://doi.org/10.1038/nature09454.
[14] K.T. Flaherty, C. Robert, P. Hersey, P. Nathan, C. Garbe, M. Milhem, L.V. Demidov, J.C. Hassel, P. Rutkowski, P. Mohr, R. Dummer, U. Trefzer, J.M. Larkin, J. Utikal, B. Dreno, M. Nyakas, M.R. Middleton, J.C. Becker, M. Casey, L. J Sherman, F.S. Wu, D. Ouellet, A.M. Martin, K. Patel, D. Schadendorf, METRIC Study Group, Improved survival with MEK inhibition in BRAF-mutated melanoma N, Engl. J. Med. 367 (2012) 107–114, https://doi.org/10.1056/NEJMoa1203421.
[15] D.B. Solit, N. Rosen, Resistance to BRAF inhibition in melanomas, N. Engl. J. Med. 364 (2011) 772–774, https://doi.org/10.1056/NEJMcibr1013704.
[16] J.J. Luke, F.S. Hodi, Ipilimumab, vemurafenib, dabrafenib, and trametinib: synergistic competitors in melanoma, Oncol. 18 (2013) 717–725, https://doi.org/10.1634/theoncologist.2012-0391.
[17] F.S. Hodi, S.J. O'Day, D.F. McDermott, R.W. Weber, J.A. Sosman, J.B. Haanen, R. Gonzalez, C. Robert, D. Schadendorf, J.C. Hassel, W. Akerley, A.J. van den Eertwegh, J. Lutzky, P. Lorigan, J.M. Vaubel, G.P. Linette, D. Hogg, C.H. Ottensmeier, C. Lebbé, C. Peschel, I. Quirt, J.I. Clark, J.D. Wolchok, J.S. Weber, J. Tian, M.J. Yellin, G.M. Nichol, A. Hoos, W.J. Urba, Improved survival with ipilimumab in patients with metastatic melanoma, N. Engl. J. Med. 363 (2010) 711–723, https://doi.org/10.1056/NEJMoa1003466.
[18] S. Topalian, M. Sznol, D.F. McDermott, H.M. Kluger, R.D. Carvajal, W.H. Sharfman, J.R. Brahmer, D.P. Lawrence, M.B. Atkins, J.D. Powderly, P.D. Leming, E.J. Lipson, I. Puzanov, D.C. Smith, J.M. Taube, J.M. Wigginton, G.D. Kollia, A. Gupta, D.M. Pardoll, J.A. Sosman, F.S. Hodi, Survival, durable tumor remission, and long-term safety in patients with advanced melanoma receiving nivolumab, J. Clin. Oncol. 32 (2014) 1020–1030, https://doi.org/10.1200/JCO.2013.53.0105.
[19] G.A. McArthur, P.B. Chapman, C. Robert, J. Larkin, J.B. Haanen, R. Dummer, A. Ribas, D. Hogg, O. Hamid, P.A. Ascierto, C. Garbe, A. Testori, M. Maio, P. Lorigan, C. Lebbé, T. Jouary, D. Schadendorf, S.J. O'Day, J.M. Kirkwood, A.M. Eggermont, B. Dréno, J.A. Sosman, K.T. Flaherty, M. Yin, I. Caro, S. Cheng, K. Trunzer, A. Hauschild, Safety and efficacy of vemurafenib in BRAFV600E and BRAFV600K mutation-positive melanoma (BRIM-3): extended follow-up of a phase 3 randomised, opne-label study, Lancet Oncol. 15 (2014) 323–332, https://doi.org/10.1016/S1470-2045(14)70012-9.
[20] J.S. Weber, K.C. Kahler, A. Hauschild, Management of immune-related adverse events and kinetics of response with ipilimumab, J. Clin. Oncol. 30 (2012) 2691–2697, https://doi.org/10.1200/JCO.2012.41.6750.
[21] J. Larkin, V. Chiarion-Sileni, R. Gonzalez, J.J. Grob, C.L. Cowey, C.D. Lao, D. Schadendorf, R. Dummer, M. Smylie, P. Rutkowski, P.F. Ferrucci, A. Hill, J. Wagstaff, M.S. Carlino, J.B. Haanen, M. Maio, I. Marquez-Rodas, G.A. McArthur, P.A. Ascierto, G.V. Long, M.K. Callahan, M.A. Postow, K. Grossmann, M. Sznol, B. Dreno, L. Bastholt, A. Yang, L.M. Rollin, C. Horak, F.S. Hodi, J.D. Wolchok, Combined nivolumab and ipilimumab or monotherapy in untreated melanoma, N. Engl. J. Med. 373 (2015) 23–34, https://doi.org/10.1056/NEJMoa1504030.
[22] E. Valeur, S.M. Guéret, H. Adihou, R. Gopalakrishnan, M. Lemurell, H. Waldmann, T.N. Grossmann, A.T. Plowright, New modalities for challenging targets in drug discovery, Angew. Chem. Int. Ed. 56 (2017) 10294–10323, https://doi.org/10.1002/anie.201611914.
[23] S. Katsamakas, T. Chatzisideri, S. Thysiadis, V. Sarli, RGD-mediated delivery of small-molecule drugs, Future Med. Chem. 9 (2017) 579–604, https://doi.org/10.4155/fmc-2017-0008.
[24] F. Zanardi, P. Burreddu, G. Rassu, L. Auzzas, L. Battistini, C. Curti, A. Sartori, G. Nicastro, G. Menchi, N. Cini, A. Bottoncetti, S. Raspanti, G. Casiraghi, Discovery of subnanomolar arginine-glycine-aspartate-based alphaVbeta3/alphaVbeta5 integrin binders embedding 4-aminoproline residues, J. Med. Chem. 51 (2008) 1771–1782, https://doi.org/10.1021/jm701214z.
[25] L. Battistini, P. Burreddu, P. Carta, G. Rassu, L. Auzzas, C. Curti, F. Zanardi, L. Manzoni, E.M. Araldi, C. Scolastico, G. Casiraghi, 4-Aminoproline-based arginine-glycine-aspartate integrin binders with exposed ligation points: practical in-solution synthesis, conjugation and binding affinity evaluation, Org. Biomol. Chem. 7 (2009) 4924–4935, https://doi.org/10.1039/b914836a.
[26] M. Pilkington-Miksa, D. Arosio, L. Battistini, L. Belvisi, M. De Matteo, F. Vasile, P. Burreddu, P. Carta, G. Rassu, P. Perego, N. Carenini, F. Zunino, M. De Cesare, V. Castiglioni, E. Scanziani, C. Scolastico, G. Casiraghi, F. Zanardi, L. Manzoni, Design, synthesis, and biological evaluation of novel cRGD-paclitaxel conjugates for integrin-assisted drug delivery, Bioconjug. Chem. 23 (2012) 1610–1622, https://doi.org/10.1021/bc300164t.
[27] A. Sartori, F. Bianchini, S. Migliari, P. Burreddu, C. Curti, F. Vacondio, D. Arosio, L. Ruffini, G. Rassu, L. Calorini, A. Pupi, F. Zanardi, L. Battistini, Synthesis and preclinical evaluation of a novel, selective 111In-labelled aminoproline-RGD-peptide for non-invasive melanoma tumor imaging, MedChemComm 6 (2015) 2175–2183, https://doi.org/10.1039/C5MD00301F.
[28] A. Sartori, E. Portioli, L. Battistini, L. Calorini, A. Pupi, F. Vacondio, D. Arosio, F. Bianchini, F. Zanardi, Synthesis of novel c(AmpRGD)-sunitinib dual conjugates as molecular tools targeting the α(v)β(3) integrin/VEGFR2 couple and impairing tumor-associated angiogenesis, J. Med. Chem. 60 (2017) 248–262, https://doi.org/10.1021/acs.jmedchem.6b01266.
[29] J.S. Desgrosellier, D.A. Cheresh, Integrins in cancer: biological implications and therapeutic opportunities, Nat. Rev. Canc. 10 (2010) 9–22, https://doi.org/10.1038/nrc2748.
[30] S. Baka, A.R. Clamp, G.C. Jayson, A review of the latest clinical compounds to inhibit VEGF in pathological angiogenesis, Expert Opin. Ther. Targets 10 (2006) 867–876, https://doi.org/10.1517/14728222.10.6.867.
[31] C. Le Tourneau, E. Raymond, S. Faivre, Sunitinib: a novel tyrosine kinase inhibitor. A brief review of its therapeutic potential in the treatment of renal carcinoma and gastrointestinal stromal tumors (GIST), Ther. Clin. Risk Manag. 3 (2007) 341–348, https://doi.org/10.2147/tcrm.2007.3.2.341.
[32] M.P. Sablin, C. Dreyer, C. Colichi, M. Bouattour, C. Delbaldo, S. Faivre, E. Raymond, Benefits from pharmacological and pharmacokinetic properties of sunitinib for clinical development, Expert Opin. Drug Metabol. Toxicol. 6 (2010) 1005–1015, https://doi.org/10.1517/17425255.2010.506872.
[33] Z. Hao, I. Sadek, Sunitinib: the antiangiogenic effects and beyond, OncoTargets Ther. 9 (2016) 5495–5505, https://doi.org/10.2147/OTT.S112242.
[34] A. Avdeef, pH-metric log P. II: refinement of partition coefficients and ionization constants of multiprotic substances, J. Pharm. Sci. 82 (1993) 183–190, https://doi.org/10.1002/jps.2600820214.
[35] A. Avdeef, J.E.A. Comer, S.J. Thomson, pH-Metric log P. 3. Glass electrode calibration in methanol-water, applied to pKa determination of water-insoluble substances, Anal. Chem. 65 (1993) 42–49, https://doi.org/10.1021/ac00049a010.
[36] T.R. Chen, In situ detection of mycoplasma contamination in cell cultures by fluorescent Hoechst 33258 stain, Exp. Cell Res. 104 (1977) 255–262, https://doi.org/10.1016/0014-4827(77)90089-1.
[37] V. Maggi, F. Bianchini, E. Portioli, S. Peppicelli, M. Lulli, D. Bani, R. Del Sole, F. Zanardi, A. Sartori, R. Fiammengo, Gold nanoparticles functionalized with RGD-semipeptides: a simple yet highly effective targeting system for αVβ3 integrins, Chem. Eur J. (2018), https://doi.org/10.1002/chem.201801823.
[38] L. Sernissi, A. Trabocchi, D. Scarpi, F. Bianchini, E.G. Occhiato, Cyclic RGD peptidomimetics containing 4- and 5-amino-cyclopropane pipecolic acid (CPA) templates as dual αVβ3 and α5β1 integrin ligands, Bioorg. Med. Chem. 15 (2016) 703–711, https://doi.org/10.1016/j.bmc.2015.12.039.
[39] C.P. Popolin, J.P.B. Reis, A.B. Becceneri, A.E. Graminha, M.A.P. Almeida, R.S. Corrêa, L.A. Colina-Vegas, J. Ellena, A.A. Batista, M.R. Cominetti, Cytotoxicity and anti-tumor effects of new ruthenium complexes on triple negative breast cancer cells, PLoS One 12 (2017) e0183275, https://doi.org/10.1371/journal.pone.0183275.
[40] V. Carloni, M. Lulli, S. Madiai, T. Mello, A. Hall, T.V. Luong, M. Pinzani, K. Rombouts, A. Galli, CHK2 overexpression and mislocalisation within mitotic structures enhances chromosomal instability and hepatocellular carcinoma progression, Gut 67 (2017) 348–361, https://doi.org/10.1136/gutjnl-2016-313114.

[41] A. Lupia, S. Peppicelli, E. Witort, F. Bianchini, V. Carloni, N. Pimpinelli, C. Urso, L. Borgognoni, S. Capaccioli, L. Calorini, M. Lulli, CD63 tetraspanin is a negative driver of epithelial-to-mesenchymal transition in human melanoma cells, J. Invest. Dermatol. 134 (2014) 2947–2956, https://doi.org/10.1038/jid.2014.258.
[42] Y. Tanaka, M.A. Shibata, J. Morimoto, Y. Otsuki, Sunitinib suppresses tumor growth and metastases in a highly metastatic mouse mammary cancer model, Anticancer Res. 31 (2011) 1225–1234 PMID: 21508369.
[43] S. Albelda, Integrins and other cell adhesion molecules, FASEB J. 4 (1990) 2868–2880 PMID: 2199285.
[44] P. Natali, Clinical significance of alpha(v)beta3 integrin and intercellular adhesion molecule-1 expression in cutaneous malignant melanoma lesions, Cancer Res. 57 (1997) 1554–1560 PMID: 9108459.
[45] E. Danen, Alpha v-integrins in human melanoma: gain of alpha v beta 3 and loss of alpha v beta 5 are related to tumor progression in situ but not to metastatic capacity of cell lines in nude mice, Int. J. Canc. 61 (1995) 491–496 PMID: 7538977.
[46] T. Vlaykova, P. Laurila, T. Muhonen, M. Hahka-Kemppinen, A. Jekunen, K. Alitalo, S. Pyrhönen, Prognostic value of tumour vascularity in metastatic melanoma and association of blood vessel density with vascular endothelial growth factor expression, Melanoma Res. 9 (1999) 59–68 PMID: 10338335.
[47] S. Ugurel, G. Rappl, W. Tilgen, U. Reinhold, Increased serum concentration of angiogenic factors in malignant melanoma patients correlates with tumor progression and survival, J. Clin. Oncol. 19 (2001) 577–583, https://doi.org/10.1200/JCO.2001.19.2.577.
[48] J. Graells, A. Vinyals, A. Figueras, A. Llorens, A. Moreno, J. Marcoval, F.J. Gonzalez, A. Fabra, Overproduction of VEGF concomitantly expressed with its receptors promotes growth and survival of melanoma cells through MAPK and PI3K signaling, J. Invest. Dermatol. 123 (2004) 1151–1161, https://doi.org/10.1111/j.0022-202X.2004.23460.x.
[49] F. Hodi, Bevacizumab plus ipilimumab in patients with metastatic melanoma, Cancer Immunol. Res. 2 (2014) 632–642, https://doi.org/10.1158/2326-6066.CIR-14-0053.
[50] A. Imbulgoda, D.Y. Heng, C. Kollmannsberger, Sunitinib in the treatment of advanced solid tumors, Recent Results Canc. Res. 201 (2014) 165–184 PMID:24756791.
[51] G. Aparicio-Gallego, M. Blanco, A. Figueroa, R. García-Campelo, M. Valladares-Ayerbes, E. Grande-Pulido, L. Antón-Aparicio, New insights into molecular mechanisms of sunitinib-associated side effects, Mol. Canc. Therapeut. 10 (2011) 2215–2223, https://doi.org/10.1158/1535-7163.MCT-10-1124.
[52] S.F. Mulder, D. Bertens, I.M. Desar, K.C. Vissers, P.F. Mulders, C.J. Punt, D.J. van Spronsen, J.F. Langenhuijsen, R.P. Kessels, C.M. van Herpen, Impairment of cognitive functioning during Sunitinib or Sorafenib treatment in cancer patients: a cross sectional study, BMC Canc. 14 (2014) 219, https://doi.org/10.1186/1471-2407-14-219.
[53] M.E. Valsecchi, T. Sato, The potential role of sunitinib targeting melanomas, Expert Opin. Investig. Drugs 22 (2013) 1473–1483, https://doi.org/10.1517/13543784.2013.837449.
[54] X. Kuang, M. Qi, C. Peng, C. Zhou, J. Su, W. Zeng, H. Liu, J. Zhang, M. Chen, M. Shen, X. Xie, F. Li, S. Zhao, Q. Li, Z. Luo, J. Chen, J. Tao, Y. He, X. Chen, Propranolol enhanced the anti-tumor effect of sunitinib by inhibiting proliferation and inducing G0/G1/S phase arrest in malignant melanoma, Oncotarget 9 (2017) 802–811, https://doi.org/10.18632/oncotarget.22696.
[55] D.R. Minor, M. Kashani-Sabet, M. Garrido, S.J. O'Day, O. Hamid, B.C. Bastian, Sunitinib therapy for melanoma patients with KIT mutations, Clin. Canc. Res. 18 (2012) 1457–1463, https://doi.org/10.1158/1078-0432.CCR-11-1987.
[56] S. Harmsen, M.E.M. Dolman, Z. Nemes, M. Lacombe, B. Szokol, J. Pató, G. Kéri, L. Őrfi, G. Storm, W.E. Hennink, R.J. Kok, Bioconjug. Chem. 22 (2011) 540–545, https://doi.org/10.1021/bc1005637.
[57] M.E.M. Dolman, S. Harmsen, E.H.E. Pieters, R.W. Sparidans, M. Lacombe, B. Szokol, L. Orfi, G. Kéri, G. Storm, W.E. Hennink, R.J. Kok, Targeting a platinum-bound sunitinib analog to renal proximal tubular cells, Int. J. Nanomed. 7 (2012) 417–433, https://doi.org/10.2147/IJN.S26485.
[58] G.T. Noh, M.H. Kim, J.Y. Suh, Y. Song, C.K. Lee, J.H. Baek, Y.S. Lee, G. Cho, E. Kim, Y.R. Kim, H.J. Cho, D. Lim, J.K. Kim, Sunitinib-CLIO conjugate: a VEGFR/PDGFR-targeting active MR probe, Mol. Imag. Biol. 16 (2014) 340–349, https://doi.org/10.1007/s11307-013-0697-9.
[59] O. Argyros, T. Karampelas, X. Asvos, A. Varela, N. Sayyad, A. Papakyriakou, C.H. Davos, A.G. Tzakos, D. Fokas, C. Tamvakopoulos, Peptide-drug conjugate GnRH-sunitinib targets angiogenesis selectively at the site of action to inhibit tumor growth, Cancer Res. 76 (2016) 1181–1192, https://doi.org/10.1158/0008-5472.CAN-15-2138.
[60] J.A. Kemp, M.S. Shim, C.Y. Heo, Y.J. Kwon, Combo" nanomedicine: Co-delivery of multi-modal therapeutics for efficient, targeted, and safe cancer therapy, Adv. Drug Deliv. Rev. 98 (2016) 3–18, https://doi.org/10.1016/j.addr.2015.10.019.
[61] K.J. Gotink, H.J. Broxterman, M. Labots, R.R. de Haas, H. Dekker, R.J. Honeywell, M.A. Rudek, L.V. Beerepoot, R.J. Musters, G. Jansen, A.W. Griffioen, Y.G. Assaraf, R. Pili, G.J. Peters, H.M. Verheul, Lysosomal sequestration of sunitinib: a novel mechanism of drug resistance, Clin. Canc. Res. 17 (2011) 7337–7346, https://doi.org/10.1158/1078-0432.CCR-11-1667.
[62] P. Marzola, A. Degrassi, L. Calderan, P. Farace, E. Nicolato, C. Crescimanno, M. Sandri, A. Giusti, E. Pesenti, A. Terron, A. Sbarbati, F. Osculati, Early anti-angiogenic activity of SU11248 evaluated *in vivo* by dynamic contrast-enhanced magnetic resonance imaging in an experimental model of colon carcinoma, Clin. Canc. Res. 11 (2005) 5827–5832, https://doi.org/10.1158/1078-0432.CCR-04-2655.
[63] K.J. Gotink, H.J. Broxterman, R.J. Honeywell, H. Dekker, R.R. de Haas, K.M. Miles, R. Adelaiye, A.W. Griffioen, G.J. Peters, R. Pili, H.M. Verheul, Acquired tumor cell resistance to sunitinib causes resistance in a HT-29 human colon cancer xenograft mouse model without affecting sunitinib biodistribution of the tumor microvasculature, Oncoscience 1 (2014) 844–853, https://doi.org/10.18632/oncoscience.106.
[64] H.K. Shete, R.H. Prabhu, V.B. Patravale, Endosomal escape: a bottleneck in intracellular delivery, J. Nanosci. Nanotechnol. 14 (2014) 460–474 PMID: 24730275.
[65] B. Speed, H.-Z. Bu, W.F. Pool, G.W. Peng, E.Y. Wu, S. Patyna, C. Bello, P. Kang, Pharmacokinetics, distribution, and metabolism of [14C]sunitinib in rats, monkeys, and humans, Drug Metab. Dispos. 40 (2012) 539–555, https://doi.org/10.1124/dmd.111.042853.